Eur. Phys. J. Spec. Top. (2021) 230:505–515
https://doi.org/10.1140/epjs/s11734-021-00002-6

THE EUROPEAN PHYSICAL JOURNAL SPECIAL TOPICS

Regular Article

Supernova neutrino detection through neutron emission by nuclei

Pijushpani Bhattacharjee[1,a] and Kamales Kar[2,b]

[1] Saha Institute of Nuclear Physics, 1/AF Bidhannagar, Kolkata 700064, India
[2] Ramakrishna Mission Vivekananda Educational and Research Institute, Belur Math, Howrah 711202, India

Received 7 April 2020 / Accepted 23 December 2020 / Published online 29 March 2021

Abstract Neutrinos from core collapse supernovae can excite nuclei of some detector materials beyond their neutron emission thresholds. Detection of these neutrons can give valuable information about the supernova explosion mechanism and possibly also throw light on neutrino properties. In this article, we give a brief review of the basic physics of neutrino-induced neutron emission and describe the results of some recent calculations of supernova neutrino-induced neutrons for some specific target detector materials due to charged current (CC) interactions of the electron flavored neutrinos and antineutrinos as well as due to neutral current (NC) interactions of neutrinos and antineutrinos of all flavors with the detector nuclei. We highlight the fact that a detector material such as lead with a relatively large neutron excess produces neutrons dominantly through the CC interaction of the ν_es, whereas a material such as iron with small neutron excess produces neutrons dominantly through the combined NC interaction of all the six neutrino and antineutrino species. This raises the interesting possibility of probing the fraction of mu- and tau-flavored neutrinos (which interact only through NC interaction) in the supernova neutrino flux by means of simultaneous detection of a supernova in a lead and an iron detector, for example.

1 Introduction

The explosion of core collapse supernovae (SN) is associated with the emission of a huge number of neutrinos [1–3]. These neutrinos come out from the central very high density region of the core of the star and are the only messengers of the conditions there [4,5]. The detection of neutrinos from SN 1987A has provided direct observational evidence for neutrino emission from supernovae. But the number of neutrinos observed was very small—a total of 20 events over a period of slightly less than 13 s at the two water Cerenkov facilities, Kamiokanda-II [6] and Irvine–Michigan–Brookhaven (IMB) [7]. However, today there exist many excellent neutrino detectors, like the Cerenkov or liquid scintillator facilities such as Super-Kamiokande [8], IceCube [9], Borexino [10], KamLAND [11,12], LVD [13], RENO-50 [14], and future ones like IceCube-Gen2 [15], Hyper-Kamiokande [16] and JUNO [17], which will be able to detect copious number of neutrinos from a future nearby supernova event. While these observe the electron antineutrinos, the liquid argon detector within the DUNE facility [18] will observe the electron neutrinos.

In this article, we discuss another mechanism of SN neutrino detection, namely through detection of neutrino induced neutrons with suitably chosen detector materials. Supernova neutrinos and antineutrinos interacting with some nuclei can excite the nuclei beyond their neutron emission thresholds, resulting in emission of neutrons. Neutrinos and antineutrinos of all flavors participate in the neutral current (NC) excitation process, whereas the electron flavor neutrinos can additionally excite the nuclei through the charged current (CC) interaction. These neutrons detected in coincidence with the SN event can give valuable information about the energy spectra of the supernova neutrinos. Detectors for this purpose can in principle employ a variety of detector materials such as lead [19] (as in the HALO [20] experiment at SNOLAB), iron [21,22], liquid xenon [23], and so on. The total number of neutrons emitted due to CC interactions of ν_es with a nucleus ${}^{A}_{Z}\mathrm{X}$ of mass number A with Z protons and $N(=A-Z)$ neutrons roughly scales with the "neutron excess" $(=N-Z)$ of the nucleus. Thus, ${}^{208}_{82}\mathrm{Pb}$ or ${}^{132}_{54}\mathrm{Xe}$, for example, with 'large' and 'moderate' neutron excesses of 44 and 24, respectively, will respond more to electron type neutrinos than the mu or tau type. However, materials with low neutron excess ($N \approx Z$), such as ${}^{56}\mathrm{Fe}$ (with $N=30$, $Z=26$), for example, can also be useful since such materials can be relatively more sensitive to ν_μ and ν_τ and their antineutrinos (all of which only have NC interactions with the nuclei) because of the suppression of CC interactions of electron type neutrinos. As we shall see below, the total number of neu-

[a] e-mail: pijush.bhattacharjee@saha.ac.in (corresponding author)
[b] e-mail: kamales.kar@gm.rkmvu.ac.in

trons emitted also differs for the two different neutrino mass hierarchies, namely, Normal Ordering (NO) and Inverted Ordering (IO).

In Sect. 2, we briefly review the general features of the neutrinos emitted during core collapse supernovae. Section 3 discusses the excitation of nuclei by neutrinos carrying energies in the range of a few to few tens of MeV, both for CC and NC interactions, and the process of neutron emission. In Sect. 4, we discuss three specific detector materials, namely, ^{56}Fe, ^{132}Xe and ^{208}Pb (covering the range of 'low' through 'intermediate' to 'heavy' mass nuclei) with regard to their effectiveness for neutrino-induced neutron emission, and present some results for these materials in Sect. 5. Finally, in Sect. 6, we summarize and mention possible future work in this area.

2 Neutrinos from core collapse supernovae

Detailed numerical simulations with realistic physics allow one to model the fluxes and energies of neutrinos emitted during the core collapse supernovae. The emission of neutrinos can be separated into three distinct phases. Electron capture on nuclei $^{A}\mathrm{X}_{N}$ and on the free protons (p) result in neutrino production when the shock wave responsible for the explosion passes through the iron core, dissociating the iron nuclei while moving outward. This phase, known as the neutronization phase, lasts for 25–30 ms and gives out predominantly electron type neutrinos (ν_e) :

$$^{A}\mathrm{X}_{N} + e^{-} \rightarrow {}^{A}\mathrm{Y}_{N+1} + \nu_e, \quad (1)$$

$$p + e^{-} \rightarrow n + \nu_e. \quad (2)$$

After this, in the accretion phase, which lasts for a few hundred milliseconds, neutrinos of all flavors are emitted. As the infalling material accretes onto the core, the matter gets sufficiently heated so that the $e^{+}e^{-}$ annihilation process results in $\nu\bar{\nu}$ production of all three neutrino flavors. The nucleon–nucleon bremsstrahlung, $NN' \rightarrow NN' + \nu\bar{\nu}$, also adds to that. The ν_e and $\bar{\nu}_e$ are produced through both CC and NC processes whereas the ν_μ, $\bar{\nu}_\mu$, ν_τ and $\bar{\nu}_\tau$ are produced only through NC processes. The ν_μ, $\bar{\nu}_\mu$, ν_τ and $\bar{\nu}_\tau$ have identical flux and energy distributions. At the final stage neutrinos come out during the cooling phase which lasts for about 10 s during which the fluxes go down with time. The fluxes and average energies of ν_e, $\bar{\nu}_e$ and ν_x (where ν_x represents ν_μ , $\bar{\nu}_\mu$, ν_τ or $\bar{\nu}_\tau$) as functions of time for all the three stages from the results of a realistic simulation by the Basel/Darmstadt (B/D) group [24] are shown in Fig. 1 for illustration.

The average neutrino energies obtained in the B/D simulations [24] are somewhat lower than those from earlier simulations [25,26]. In the last few years, there has been progress in the inclusion of mean-field effects modifying the nuclear symmetry energy for the CC interaction [27], which goes towards reducing the luminosities of all neutrino flavors but increases the difference between the ν_e's and $\bar{\nu}_e$'s average energies. There is also better understanding of the medium modification for neutrino-pair processes from nucleon–nucleon bremsstrahlung, which modifies the process of deleptonization of the protoneutron star [28]. In this article, we shall use for definiteness the temporal profiles of the neutrino luminosities and average energies of the neutrinos of different flavors as well as their normalized time-averaged energy spectra given by the Basel/Darmstadt simulation [24] of a $18\,\mathrm{M}_{\odot}$ progenitor supernova (as shown in Fig. 1) at a distance of 10 kpc from earth, for illustrating our results for neutron emission in different detector materials.

The post-bounce differential flux (per unit time per unit energy) of each neutrino flavor ν_i ($\nu_i \equiv \nu_e, \bar{\nu}_e, \nu_x$) at time t is written as

$$F^{0}_{\nu_i}(t, E_\nu) = \frac{L_{\nu_i}(t)}{\langle E_{\nu_i}\rangle(t)} \varphi_{\nu_i}(E_\nu, t), \quad (3)$$

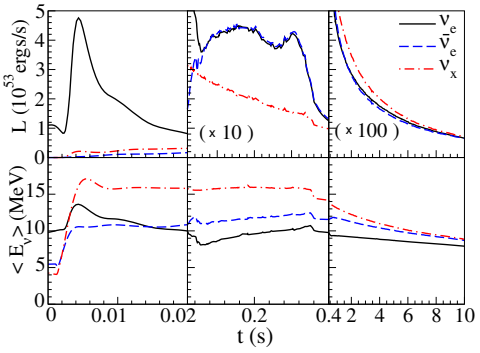

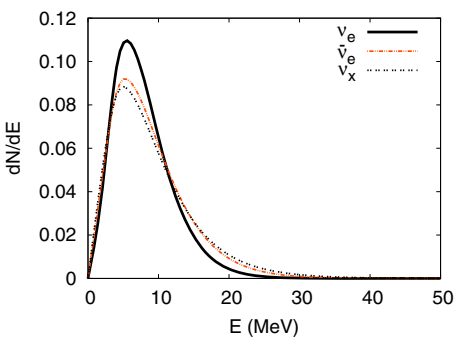

Fig. 1 Left: Temporal profiles of the neutrino luminosity (upper three panels) and average energy of the neutrinos (lower three panels) during the neutronization-, accretion- and cooling phase (from left to right, respectively) for different neutrino flavors, as given by the Basel/Darmstadt simulation [24] of a $18\,\mathrm{M}_{\odot}$ progenitor supernova. Here ν_x represents ν_μ , $\bar{\nu}_\mu$, ν_τ or $\bar{\nu}_\tau$. Right: The normalized time-averaged energy spectra of the neutrinos of different flavors. (From Ref. [22])

where $L_{\nu_i}(t)$ and $\langle E_{\nu_i}\rangle(t)$ are the time-dependent luminosity and average energy of the emitted neutrinos of flavor ν_i, and $\varphi_{\nu_i}(E_\nu, t)$ is the instantaneous normalized energy spectrum ($\int \varphi_{\nu_i}(E_\nu, t)\mathrm{d}E_\nu = 1$), which can be parametrized as [26]

$$\varphi_{\nu_i}(E_\nu, t) = \frac{1}{\langle E_{\nu_i}\rangle(t)} \frac{\Big(1+\alpha_{\nu_i}(t)\Big)^{1+\alpha_{\nu_i}(t)}}{\Gamma\Big(1+\alpha_{\nu_i}(t)\Big)} \left(\frac{E_\nu}{\langle E_{\nu_i}\rangle(t)}\right)^{\alpha_{\nu_i}(t)} \times \exp\left[-\Big(1+\alpha_{\nu_i}(t)\Big)\frac{E_\nu}{\langle E_{\nu_i}\rangle(t)}\right], \tag{4}$$

where

$$\alpha_{\nu_i}(t) = \frac{2\langle E_{\nu_i}\rangle^2(t) - \langle E^2_{\nu_i}\rangle(t)}{\langle E^2_{\nu_i}\rangle(t) - \langle E_{\nu_i}\rangle^2(t)}$$

is the spectral shape parameter.

It is now well established that at least two of the three active neutrino species have small but non-zero masses and the probability of finding a neutrino with a specific flavor oscillates as it moves [29]. These vacuum oscillation probabilities depend on the mass squared differences and the flavor mixing angles. With the mass eigenstates having masses m_1, m_2 and m_3, solar neutrino deficit measurements give estimates of Δm^2_{12} ($\equiv m^2_2 - m^2_1$) > 0 while the resolution of the atmospheric neutrino anomaly gives information on the value of $|\Delta m^2_{23}|$ (with $\Delta m^2_{23} \equiv m^2_3 - m^2_2$), but not its sign. So one unsolved problem of neutrino physics is whether $m_3 > m_2$ (Normal Ordering (NO)), or $m_3 < m_2$ (Inverse Ordering (IO)).

The vacuum oscillations get enhanced in presence of matter, an effect known as the Mikheyev–Smirnov–Wolfenstein (MSW) effect [29]. For neutrinos moving through matter with a density gradient a resonance in the oscillations can take place. The neutrinos can have the resonance for NO but not for IO and similarly the antineutrinos can have the resonance for IO, but not for NO.

For core collapse supernovae, the matter density goes through a large gradient from the central region to the edge of the core. Generally, one encounters two densities where resonances can take place [30] and so the luminosities of the different neutrino flavors depend on the mass ordering (NO or IO). So the flux of neutrinos reaching the detector is different for different mass ordering. In addition, of course, the flux of neutrinos reaching the earth has the factor of $1/(4\pi d^2)$, where d is the distance of the supernova from the earth.

On top of the matter-enhanced oscillations, there can be oscillations due to neutrino–neutrino interaction or neutrino self-interaction, an effect known as collective oscillations [31,32]. This happens only at regions with very high neutrino densities in the region of a few hundred kms from centre of the core during the accretion phase at a post-bounce time $t_{\rm pb} < 0.5$ s. This results in multiple splits in the neutrino spectra. This pre-processes the fluxes of the neutrinos before they move into the MSW region. However, as the net electron density in this collective oscillation region is not small, one sees that large matter-induced phase dispersion for neutrinos traveling in different directions partially or totally suppresses the collective oscillations [33]. Detailed numerical simulations [34,35] observed this suppression using results of SN hydrodynamic simulations. On the other hand, in the cooling phase, the matter suppression is not present anymore and collective effects should take place before the neutrinos enter the regions of lower densities. But in the cooling phase, the neutrino fluxes of different flavors are very similar and the effects of such oscillations on them are not important from the observational point of view. So, for simplicity, in this article, we ignore the collective oscillation effect and consider only the MSW oscillation effects.

3 Nuclear excitations by neutrinos and emission of neutrons

Charged current interaction of a SN ν_e with a detector nucleus ${}^A_Z\mathrm{X}_N$ can produce the nucleus ${}^A_{Z+1}\mathrm{Y}_{N-1}$ which, depending on the incident ν_e energy, can be produced in an excited state (denoted by a superscript $*$):

$$\nu_e + {}^A_Z\,\mathrm{X}_N \rightarrow e^- + {}^A_{Z+1}\mathrm{Y}^*_{N-1}, \tag{5}$$

with subsequent de-excitation of the final state nucleus through emission of various particles (γ, p, n, α, and so on) depending on the excitation energy of the nucleus. We are interested in the situation when the nucleus de-excites by emitting one or more neutrons:

$${}^A_{Z+1}\mathrm{Y}^*_{N-1} \rightarrow {}^{A-1}_{Z+1}\mathrm{Y}_{N-2} + n, \tag{6}$$

$${}^A_{Z+1}\mathrm{Y}^*_{N-1} \rightarrow {}^{A-2}_{Z+1}\mathrm{Y}_{N-3} + 2n, \tag{7}$$

and so forth. Emission of three or more neutrons is possible in principle but their contribution to the total number of neutron emission is negligibly small as the thresholds for emission of three or more neutrons are generally very high compared to the range of energies over which the nucleus can be excited by the SN neutrinos.

Similar to ν_es, the SN $\bar{\nu}_e$s can also interact with the detector nucleus through CC interaction producing a e^+ and an excited final state nucleus:

$$\bar{\nu}_e + {}^A_Z\,\mathrm{X}_N \rightarrow e^+ + {}^A_{Z-1}\,\tilde{\mathrm{Y}}^*_{N+1}. \tag{8}$$

The final state nucleus, if excited above single, double or higher neutron emission thresholds will emit neutrons in competition with other particles. However, in this case, since the production of the final state nucleus involves conversion of a proton into a neutron inside the nucleus, the cross section for the process is strongly suppressed due to Pauli blocking of the neutron single

particle states in nuclei with moderate to large neutron excesses $(N-Z)$ that we shall consider. Contribution of $\bar{\nu}_e$'s to neutron emission is, therefore, much smaller than that due to ν_es.

Neutrinos and antineutrinos of all three flavors (ν_i) can also excite the target nucleus through the flavor blind NC process whereby the incoming ν or $\bar{\nu}$ inelastically scatters off the nucleus leaving the latter in an excited state,

$$\nu_i + {}^{A}_{Z}\mathrm{X}_N \rightarrow \nu_i + {}^{A}_{Z}\mathrm{X}^{*}_N, \tag{9}$$

with subsequent de-excitation of the final state nucleus through neutron emission. Thus NC process has contribution from all six types of neutrinos whereas CC has contribution essentially from only one.

3.1 Neutrino–nucleus charged current cross section

For the range of energies of supernova neutrinos, the ν_e CC cross section in the $q \rightarrow 0$ limit (q being the momentum transfer) is dominated by the two allowed transitions, (a) the Fermi transition (given by $\sum_i \tau_+(i)$, where τ_+ is the operator that converts a neutron to a proton and the summation is over all the nucleons), which goes almost completely to the Isobaric Analog State (IAS) of the final nucleus, and (b) the Gamow–Teller (GT) transition (given by the operator $\sum_i \boldsymbol{\sigma}(i)\tau_+(i)$, where $\boldsymbol{\sigma}(i)$ are the standard Pauli spin matrices representing the spin operator for the ith nucleon), which is spread over a broad resonance over many final states with overlapping strengths, with some small part going to a few discrete low-lying states.

Thus, the ν_e CC differential cross section in the $q \rightarrow 0$ limit can be written as [36–38]

$$\frac{\mathrm{d}\sigma^{\mathrm{CC}}_{\nu_e}}{\mathrm{d}E_*}(E_\nu, E_*) = \frac{G_F^2 \cos^2\theta_c}{\pi}\; p_e E_e F(Z+1, E_e) \left[S_{\mathrm{F}}(E_*) + (g_{\mathrm{A}}^{\mathrm{eff}})^2 S_{\mathrm{GT}_-}(E_*)\right], \tag{10}$$

where G_F is the Fermi constant, θ_c is the Cabibbo angle, p_e and E_e are the momentum and energy of the emitted electron, $E_* = E_\nu - E_e$ is the excitation energy of the final nucleus, and $S_{\mathrm{F}}(E_*)$ and $S_{\mathrm{GT}_-}(E_*)$ are, respectively, the averaged Fermi and Gamow–Teller (GT_-) matrix elements between the ground state of the initial nucleus ${}^{A}_{Z}\mathrm{X}_N$ and the excited state (at energy E_*) of the final nucleus ${}^{A}_{Z+1}\mathrm{Y}^{*}_{N-1}$:

$$S_{\mathrm{F}}(E_*) = \frac{1}{2J_i+1}\left|\left\langle J_f \| \sum_{k=1}^{A} \tau_+(k) \| J_i \right\rangle\right|^2 \tag{11}$$

and

$$S_{\mathrm{GT}_-}(E_*) = \frac{1}{2J_i+1}\left|\left\langle J_f \| \sum_{k=1}^{A} \tau_+(k)\boldsymbol{\sigma}(k) \| J_i \right\rangle\right|^2. \tag{12}$$

The quantity $g_{\mathrm{A}}^{\mathrm{eff}} \simeq 1.26$ is the ratio of the effective axial vector to vector coupling constants of the bare nucleon in the $q \rightarrow 0$ limit [36,37]. In equation (10), the factor $F(Z+1, E_e)$, which takes into account the Coulomb distortion of the outgoing electron wave function, is given by [39]

$$F(Z,E) = 2(1+\gamma_0)(2p_eR)^{2(\gamma_0-1)} \frac{|\Gamma(\gamma_0+iy)|^2}{|\Gamma(2\gamma_0+1)|^2}\exp(\pi y), \tag{13}$$

where $\gamma_0 = (1-Z^2\alpha^2)^{1/2}$, $y = \alpha Z E_e/p_e$, R is the radius of final nucleus and α the fine structure constant.

There are also contributions from forbidden transitions ($\Delta l \neq 0$ for the single particle transitions), but normally they are one to two orders of magnitude smaller than the contributions of the allowed ones and need to be considered only when the Fermi and most of GT strengths are blocked.

Phenomenologically, it is seen that the bare nucleon value for $g_{\mathrm{A}}^{\mathrm{eff}} \simeq 1.26$ somewhat overestimates the GT strengths at low excitation energies. But since for our purpose, we are interested in the GT strengths at higher excitations beyond the neutron emission thresholds covering the whole GT resonance over tens of MeV, we think the use of the bare nucleon value for $g_{\mathrm{A}}^{\mathrm{eff}}$ is a good approximation.

The total ν_e CC cross section as a function of the incoming neutrino energy E_ν is then given by

$$\sigma^{\mathrm{CC}}_{\nu_e}(E_\nu) = \int_0^{E_\nu} \frac{\mathrm{d}\sigma^{\mathrm{CC}}_{\nu_e}}{\mathrm{d}E_*}\mathrm{d}E_*. \tag{14}$$

For the GT strength distribution, one often does theoretical calculations in model many-nucleon spaces with realistic interactions which can reproduce the observed ground state and excited state energies as well as the observed $\log ft$ values for a few low-lying states. For some nuclei forward angle (p,n) reaction gives the GT_- strengths experimentally. For comparatively lighter nuclei in the Fe–Ni region, one does a large-dimensional shell model calculation [40] or a calculation using the Shell Model Monte Carlo (SMMC) technique [41]. The strengths often sensitively depend on the interaction. For the lower part of fp-shell nuclei, the Kuo–Brown KB3 [42,43] interaction with the corrected monopole interaction is adequate. However, the upper part of the shell needs a better handling of the monopole part involving the higher orbits in the shell. But this shell model approach becomes computationally increasingly difficult as one goes to heavier nuclei. For these nuclei, like ^{208}Pb, one resorts to the RPA approach [19]. Finally, for nuclei which are not spherical in ground state region one carries out a deformed Skyrme–Hartree–Fock mean field calculation with pairing correlation in the BCS approximation [44]. The GT_- transition strengths are obtained by a quasiparticle random phase approximation (QRPA) with a residual spin-isospin interaction [45].

3.2 Neutrino–nucleus neutral current cross section

For the NC, the allowed contribution to the differential cross section for inelastic scattering involving energy transfer to the target nucleus in the $q \to 0$ limit is again governed by the corresponding GT (the so-called GT_0) strength [37], and is given by

$$\frac{\mathrm{d}\sigma^{\mathrm{NC}}_{\nu_i}}{\mathrm{d}E_*}(E_\nu, E_*) = E^2_{\nu'}\,(g^{\mathrm{eff}}_{\mathrm{A}})^2\,S_{\mathrm{GT}_0}(E_*), \tag{15}$$

where $E_{\nu'} = E_\nu - E_*$ is the energy of the final neutrino. The GT strength S_{GT_0} involves the 'z'-component of the isospin vector of the GT operator, and is given by

$$S_{\mathrm{GT}_0}(E_*) = \frac{1}{2J_i+1}\left|\left\langle J_f\right\| \sum_{k=1}^{A} \frac{1}{2}\tau_3(k)\boldsymbol{\sigma}(k)\left\|J_i\right\rangle\right|^2. \tag{16}$$

The analog of Fermi contribution in this case contributes only to the elastic part. In some cases, where energy considerations block most of the allowed strength, contributions from the much smaller forbidden transitions need to be taken into account.

The total ν_i NC cross section is obtained by integrating the differential NC cross section (15) over the excitation energy E_* of the final nucleus.

3.3 Emission of neutrons by excited nuclei

As already implicitly assumed above, the neutrino induced neutron emission from nuclei through ν_e or $\bar{\nu}_e$ CC interaction and ν_i NC inelastic scattering can be considered as a two-step process, with the final state nucleus being produced in an excited state due to absorption of energy from the incoming neutrino in the first step, and subsequent de-excitation of the nucleus through neutron emission (if the excitation energy is above the threshold for neutron emission) in the second step. The physical processes involved in these two steps can be considered to be independent of each other [19,21]. The differential cross sections for the first step, i.e., nuclear excitation through neutrino–nucleus CC or NC interaction, are given by Eqs. (10) (for ν_e) and (15), respectively. The cross section for emission of one-, two- or three neutrons, for example, by the final nucleus is then given by

$$\sigma^{\mathrm{CC(NC)}}_{1n(2n)(3n)}(E_\nu) = \int \frac{\mathrm{d}\sigma^{\mathrm{CC(NC)}}}{\mathrm{d}E_*}(E_\nu, E_*) P_{1n(2n)(3n)}(E_*)\mathrm{d}E_*, \tag{17}$$

where $\frac{\mathrm{d}\sigma^{\mathrm{CC(NC)}}}{\mathrm{d}E_*}(E_\nu, E_*)$ represents the relevant differential cross section given by Eq. (10) or (15), and $P_{1n}(E_*)$, $P_{2n}(E_*)$, $P_{3n}(E_*)$ are the probabilities for emission of one-, two- and three neutrons, respectively, by the final nucleus, as functions of the excitation energy of the final nucleus.

One can also calculate the energy spectrum of the emitted neutrons in the following way: The differential cross section for emission of neutrons per unit neutron energy E_n by a single nucleus due to an incoming neutrino of energy E_ν can be written as

$$\frac{\mathrm{d}\sigma^{\mathrm{CC(NC)}}}{\mathrm{d}E_n}(E_\nu, E_n) = \int \frac{\mathrm{d}\sigma^{\mathrm{CC(NC)}}}{\mathrm{d}E_*}(E_\nu, E_*)\frac{\mathrm{d}N_n}{\mathrm{d}E_n}(E_*, E_n)\,\mathrm{d}E_*, \tag{18}$$

where $\frac{\mathrm{d}N_n}{\mathrm{d}E_n}(E_*, E_n)$ is the energy spectrum of the neutrons produced by the excited nucleus of excitation energy E_*, with

$$\int \frac{\mathrm{d}N_n}{\mathrm{d}E_n}(E_*, E_n)\,\mathrm{d}E_n = P_{1n}(E_*) + 2\,P_{2n}(E_*) + 3\,P_{3n}(E_*), \tag{19}$$

considering up to 3-neutron emission.

The energy spectrum of all the neutrons produced by the incident flux of SN neutrinos is then given by

$$\frac{\mathrm{d}N^{\mathrm{CC(NC)}}_{n,\mathrm{total}}}{\mathrm{d}E_n} = N_0 \int \mathrm{d}E_\nu \Phi_\nu(E_\nu)\frac{\mathrm{d}\sigma^{\mathrm{CC(NC)}}}{\mathrm{d}E_n}(E_\nu, E_n), \tag{20}$$

where $\Phi_\nu(E_\nu)$ is the time-integrated flux spectrum (number per unit area per unit energy) of the SN neutrinos falling on the detector, and N_0 is the total number of target detector nuclei.

Finally, the total number of neutrons produced is given by

$$N^{\mathrm{CC(NC)}}_{n,\mathrm{total}} = \int \mathrm{d}E_n \frac{\mathrm{d}N^{\mathrm{CC(NC)}}_{n,\mathrm{total}}}{\mathrm{d}E_n} = N_0 \int \mathrm{d}E_\nu \Phi_\nu(E_\nu)\sigma^{\mathrm{CC(NC)}}_{n,\mathrm{total}}(E_\nu), \tag{21}$$

where

$$\sigma^{\mathrm{CC(NC)}}_{n,\mathrm{total}}(E_\nu) \equiv \sigma^{\mathrm{CC(NC)}}_{1n}(E_\nu) + 2\sigma^{\mathrm{CC(NC)}}_{2n}(E_\nu) + 3\sigma^{\mathrm{CC(NC)}}_{3n}(E_\nu) \tag{22}$$

with $\sigma^{\mathrm{CC(NC)}}_{1n(2n)(3n)}(E_\nu)$ given by equation (17).

The neutron emission probabilities, $P_{1n(2n)(3n)}(E_*)$, and the neutron energy spectrum, $\frac{\mathrm{d}N_n}{\mathrm{d}E_n}(E_*, E_n)$, for the desired excited nucleus can be calculated using the fusion-evaporation code PACE4 [46] originally developed by Gavron [47]. The neutron emission probabilities from excited ^{56}Fe and ^{56}Co nuclei as functions of excitation energy calculated with the PACE4 code are shown in Figs. 2 and 3, respectively, for illustration.

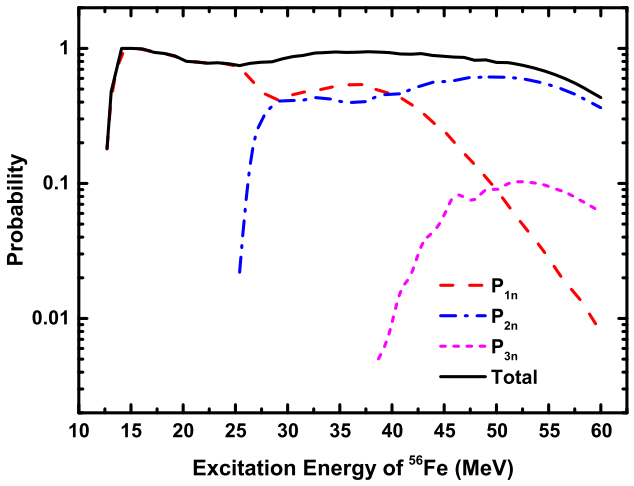

Fig. 2 The one-, two- and three-neutron emission probabilities of excited ^{56}Fe nucleus calculated with the PACE4 code [46]. (From [22])

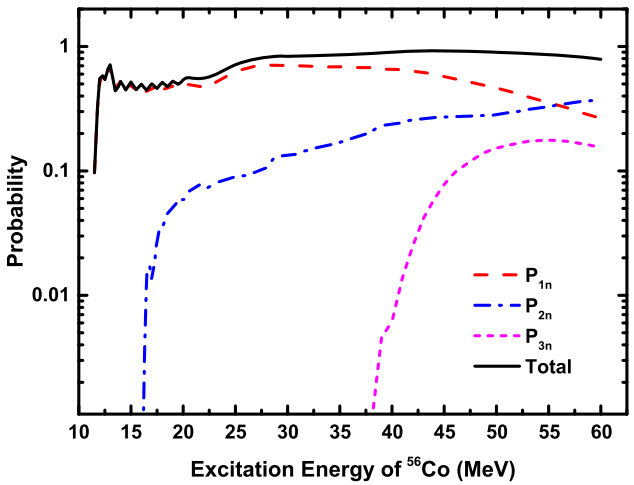

Fig. 3 The one-, two- and three-neutron emission probabilities of excited ^{56}Co nucleus calculated with the PACE4 code [46]. (From [22])

4 Neutron emission from different detector materials

The underground SNOLAB facility in the Creighton Mine in Sudbury, Canada houses a detector named HALO (Helium and Lead Observatory) [20] which is dedicated for supernova detection through detection of neutrino induced neutrons. The HALO detector consists of 79 tons of lead and uses a large number of ^{3}He neutron detectors. The element ^{208}Pb with $Z = 82$ protons has a neutron excess $(N - Z)$ of 44 and thus the total GT$_-$ strength is large as it roughly scales as $3(N - Z)$ according to Ikeda sum rule, with the GT$_+$ very small. The GT$_+$ strength coming from excitation of the nucleus by $\bar{\nu}_e$ is extremely small for ^{208}Pb as the protons need to move to states across a major shell in the shell model picture of single particle states, and so allowed GT$_+$ transitions are suppressed due to Pauli blocking. In addition, the contributions from the order of magnitude smaller forbidden transitions are also very small. For the CC reaction $^{208}\mathrm{Pb}\,(\nu_e, e^-)^{208}\mathrm{Bi}$, the excited final nucleus ^{208}Bi has one and two neutron emission thresholds at 6.89 and 14.99 MeV, respectively. As the GT$_-$ strength is a broad resonance spread over tens of MeVs, most of the Gamow–Teller transitions from ^{208}Pb and the allowed Fermi transition contribute to the process of neutron emission.

For the NC interaction $^{208}\mathrm{Pb}\,(\nu_i, \nu_i)^{208}\mathrm{Pb}$ the one and two neutron emission thresholds have comparatively low values of 7.37 and 14.11 MeV, respectively, and in this case all six neutrino species contribute. Moreover, ^{208}Pb also has a low neutron capture cross section as it is a doubly magic nucleus. Thus, the neutrons emitted from the excited nuclei resulting from both CC and NC interactions of the SN neutrinos survive while moving through the bulk detector material and are able to reach the neutron detectors.

The iron detectors with a much lighter nucleus ^{56}Fe with $Z = 26$ has the disadvantage of having a small neutron excess $(N - Z)$ of only 4, and consequently its total GT$_-$ strength is an order of magnitude smaller than in the case of lead. On top of that, for the CC reaction $^{56}\mathrm{Fe}\,(\nu_e, e^-)^{56}\mathrm{Co}$, the final ^{56}Co has the one and two neutron emission thresholds quite high at 10.08 and 24.17 MeV, respectively. So the Fermi transition to the Isobaric Analog State (IAS) gets blocked and only a part of the GT$_-$ transitions can contribute.

The total GT$_+$ strength for the process $^{56}\mathrm{Fe}\,(\bar{\nu}_e, e^+)^{56}\mathrm{Mn}$ is smaller than the total GT$_-$ strength for $^{56}\mathrm{Fe}\,(\nu_e, e^-)^{56}\mathrm{Co}$, as the valence protons of ^{56}Fe have to go to neutron single particle states at much higher energies. The total GT$_+$ strength for ^{56}Fe has the observed value of ~ 2.8 while the shell model calculations give a value of 2.7 [40]. In contrast the total GT$_-$ strength is ~ 9.9 experimentally and ~ 9.3 from theory [40]. Here again the final nucleus ^{56}Mn in the reaction $^{56}\mathrm{Fe}\,(\bar{\nu}_e, e^+)^{56}\mathrm{Mn}$ has one neutron emission threshold above 8 MeV whereas the GT$_+$ strength distribution is spread over excitation energies below 8 MeV. Hence, very little contribution comes from SN $\bar{\nu}_e$ absorption and it can be safely neglected.

Coming to intermediate mass nuclei like xenon, we note that liquid xenon scintillator detectors are already in use for dark matter (DM) detection experiments [48]. These experiments attempt to detect nuclear recoils that would be caused by the Weakly Interacting Massive Particle (WIMP) candidates of DM. However, such liquid xenon DM detectors, because of their low nuclear recoil thresholds, can also respond to supernova neutrinos [49,50] through the process of coherent elastic neutrino–nucleus scattering (CEνNS) [51–53]. At the same time, CC and NC interactions of SN neutrinos with xenon nuclei can also result in excitation of the final state nucleus, the subsequent de-excitation of which can result in emission of neutrons which can be detected through xenon nuclear recoils caused by these neutrons [23].

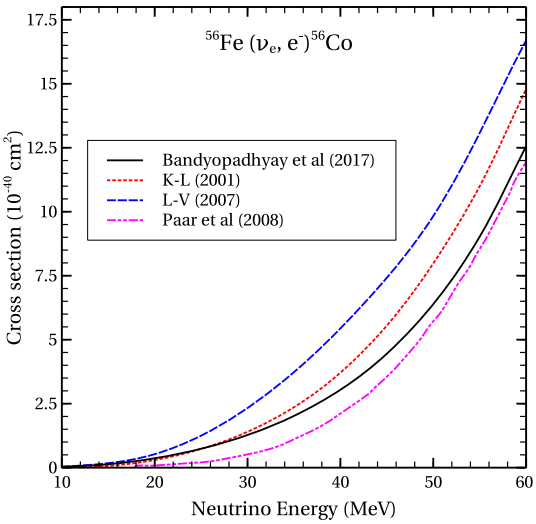

Fig. 4 Comparison of the CC cross section for the process $^{56}\mathrm{Fe}\,(\nu_e, e^-)^{56}\mathrm{Co}$ calculated in four different works, Bandyopadhyay et al. [22], Kolbe and Langanke [21] (K-L (2001)), Lazauskas and Volpe [55] (L-V (2007)), and Paar et al. [56] (Paar et al. (2008)). (From Ref. [22])

Quite a few isotopes of xenon are stable with even mass isotopes like ^{124}Xe, ^{126}Xe, ^{128}Xe, ^{130}Xe, ^{132}Xe, ^{134}Xe and ^{136}Xe having abundances 0.095%, 0.089%, 1.910%, 4.071%, 26.909%, 10.436% and 8.857%, respectively. Among the odd mass ones ^{129}Xe and ^{131}Xe have abundances of 26.40% and 21.232% respectively. In this article, we consider the example of ^{132}Xe and find its effectiveness for neutron emission after excitation by supernova neutrinos. The ^{132}Xe with $Z = 54$ has a neutron excess $(N - Z)$ of 24, and with the total GT_+ strength for the reaction $^{132}\mathrm{Xe}\,(\bar{\nu}_e, e^+)^{132}\mathrm{I}$ being very small due to Pauli blocking of single particle transitions, the GT_- total strength for the ν_e CC reaction $^{132}\mathrm{Xe}\,(\nu_e, e^-)^{132}\mathrm{Cs}$ is expected to be $\gtrsim 72\,(= 3(N-Z))$ by the Ikeda sum rule. This is indeed predicted by theoretical calculations [45] where total GT_- is obtained as 72.12 and total GT_+ as 0.51. Also the Fermi strength of 24.0 goes to the IAS in ^{132}Cs at an excitation of ~ 13.8 MeV [54]. Finally, the one and two neutron emission thresholds for the nucleus ^{132}Cs are at 7.17 and 16.40 MeV, respectively. Thus in the CC reaction on ^{132}Xe the Fermi transition and most of the GT_- transition strength contribute like in the case of ^{208}Pb.

5 Results

The ν_e CC cross section on ^{56}Fe has been calculated using the GT_- energy distribution generated by different theoretical calculations. In Fig. 4, we show a comparison of four such results where the cross section as a function of the neutrino energy is shown.

The CC cross section for $^{56}\mathrm{Fe}\,(\nu_e, e^-)^{56}\mathrm{Co}$ calculated by Bandyopadhyay et al. [22] uses the results of large dimensional shell model calculations of the GT_- strength from the 0^+ ground state of ^{56}Fe to all 1^+ states of ^{56}Co [40]. The calculations of Ref. [40] use the very successful monopole-corrected KB3 interaction [42,43]. In addition, Bandyopadhyay et al. [22] include the dominant contributions coming from the forbidden transitions to the 1^- and 2^- states of ^{56}Co. The ν_e CC cross section of this calculation agrees well with the results of Kolbe and Langanke (K-L) [21] particularly at lower energies. The K-L work for the transition strengths to 1^+ states of ^{56}Co also uses an interacting shell model calculation within the complete pf shell with an overall quenching factor of $(0.74)^2$ for the strength distribution. The results of Lazauskas and Volpe (L-V) [55] give the largest cross sections for all neutrino energies. They carry out a Hartree–Fock (HF) calculation from the ^{56}Fe ground state to the occupied single particle states using the Skyrme-type effective interaction. The unoccupied levels are obtained by diagonalizing the HF mean field using a harmonic oscillator basis. Also when needed pairing correlations are taken into account in the HF+BCS approximation. Finally in the work by Paar, Vretenar and Ring [56] the nuclear ground state is described by the relativistic Hartree–Bogoliubov model and the transition strengths to the excited levels in the relativistic quasiparticle random phase approximation (RQRPA). Their CC cross section values are lower than the ones in the other three calculations for the entire range of neutrino energy.

In Table 1, we compare the neutron emission cross sections for ^{208}Pb, ^{132}Xe and ^{56}Fe for neutrino energies in the range of SN neutrino spectra. The values for all three cases increase with the neutrino energy as the differential cross section given by Eq. (10) is proportional to the product of the electron energy and the electron momentum and their range of values increases as E_ν increases. But we see that the cross section values for ^{56}Fe are significantly smaller than those for the other two nuclei. As discussed earlier this is due to ^{56}Fe having very small neutron excess and the high neutron emission threshold of ^{56}Co blocking the contribution from the Fermi strength and a part of the GT_- strength. The intermediate mass nucleus ^{132}Xe with a neutron excess of 24 has cross sections roughly half the values for ^{208}Pb which has a neutron excess of 44. Note also that for ^{208}Pb beyond 30 MeV the 2n contribution becomes comparable to 1n values. But for ^{56}Fe the 1n contribution dominates over the 2n values over the whole range of neutrino energy considered.

Next we come to the results for the number of neutrons emitted. As already mentioned, due to neutrino flavor oscillation, the flux of SN neutrinos at earth is different for the two different neutrino mass orderings, NO and IO. As a result the numbers of neutrons emitted are also different for the two cases. Table 2 gives the number of emitted neutrons for three different detector materials, namely, ^{56}Fe, ^{132}Xe and ^{208}Pb, for CC interaction of the SN ν_es, for both NO and IO mass orderings. The numbers are for SN neutrino flux as given by the Basel/Darmstadt simulations [24] of a $18\,\mathrm{M}_\odot$ progenitor supernova at a distance of 10 kpc, and for 1

Table 1 The total neutron emission cross section, $\sigma^{\rm CC}_{n,\rm total}$ (defined by Eq. (22)), in units of 10^{-40} cm^2, for different neutrino energies due to ν_e CC interaction with ^{208}Pb (from [19]), ^{132}Xe (from [23]) and ^{56}Fe (from [22])

E_ν (MeV)	^{208}Pb	^{132}Xe	^{56}Fe
5	0.0	0.0	0.0
10	0.0	0.04	0.0
15	0.91 (0.91, 0)	0.13	0.0
20	4.96 (4.96, 0)	2.09	0.03 (0.03, 0)
25	15.56 (14.66, 0.45)	7.33	0.07 (0.07, 0)
30	31.35 (25.05, 3.15)	15.78	0.15 (0.15, 0)
35	50.97 (29.27, 10.85)	27.36	0.29 (0.28, 0.005)
40	80.92 (33.56, 23.68)	41.91	0.53 (0.49, 0.02)
45	115.85 (37.91, 38.97)	59.29	0.93 (0.85, 0.04)
50	150.12 (42.54, 53.79)	79.37	1.58 (1.40, 0.09)
55	190.43 (47.17, 71.63)	102.14	2.57 (2.23, 0.17)
60	232.12 (52.02, 90.05)	127.78	4.01 (3.43, 0.29)

These include contributions from one- and two-neutron emissions with cross sections, respectively, given within parentheses, $(\sigma^{\rm CC}_{1n}, \sigma^{\rm CC}_{2n})$, for ^{208}Pb and ^{56}Fe. (The $1n$ and $2n$ emission cross sections values for ^{132}Xe remain to be calculated.) The very small contributions from three neutron emission is neglected, so $\sigma^{\rm CC}_{n,\rm total} \approx \sigma^{\rm CC}_{1n} + 2\sigma^{\rm CC}_{2n}$. These total neutron emission cross sections, folded with the incident ν_e flux, give the total number of emitted neutrons for the chosen detector material, respectively (see Eq. (21))

kton of the given detector material. These numbers are obtained by folding the neutron emission cross sections given in Table 1 with the corresponding SN ν_e flux at earth.

As seen from Fig. 1, the spectra of the neutrinos coming from the SN core have their peaks within 10 MeV and then rapidly fall off at higher energies. The neutron numbers have their maximum in the interval of 25–30 MeV and then fall off reaching almost zero by 60 MeV. Though this neutrino energy dependence cannot be measured experimentally, they indirectly reflect the energy dependence of the source neutrinos.

The total number of emitted neutrons for ^{56}Fe, ^{132}Xe and ^{208}Pb are 3, 111 and 154, respectively, in the case of NO. Note that for ^{208}Pb one neutron comes from neutrino energies above 60 MeV and is not seen in Table 2. The numbers for the IO case for ^{56}Fe, ^{132}Xe and ^{208}Pb are 2, 83 and 117, respectively. Here again, neutrinos with energies above 60 MeV contribute 1 neutron in the case of ^{132}Xe and 2 neutrons in the case of ^{208}Pb, which are not seen in Table 2. The higher numbers for NO can be explained by the fact that for NO one has complete flavor conversion whereas for IO the conversion is partial.

The NC excitation of the nuclei is important because here all six neutrino species contribute. In Fig. 5, we present the number of neutrons emitted by 1 kton of ^{208}Pb due to NC interaction of all neutrino and antineutrino flavors with ^{208}Pb. This is given in the form of a histogram of 5 MeV energy bins for the neutrino energies. The total number of neutrons emitted is 30 with 21 coming from 1 neutron emission and 9 from the emission of 2 neutrons. The total number of NC neutrons for ^{56}Fe is about 5. Of course, NC gives identical numbers for both NO and IO because all neutrino species here contribute equally.

An interesting feature of the above results on the number of neutrons produced by different materials is to be noted: As already mentioned in Introduction, materials with large neutron excess $(N - Z)$ are expected to produce significantly more number of neutrons through ν_e CC interactions than through combined NC interactions of all the six neutrino and antineutrino species. Thus, for ^{208}Pb with a neutron excess of 44, for example, we see that only about 16% of all neutrons produced come from NC interactions and the rest come from CC interaction of the ν_es. On the other hand, in the case of ^{56}Fe with a neutron excess of only 4, more than about 60% of the produced neutrons result from NC interactions of all neutrinos. This offers an interesting complementarity between these two detector materials. Thus, simultaneous detection of a SN in a lead detector (e.g., the currently running HALO detector [20] with about 79 tons of lead) and a sufficiently large iron detector (e.g., the proposed ICAL detector [57,58] with 50 kton of iron, suitably instrumented for neutron detection[1]) may allow one to estimate the fraction of the non-electron flavored neutrinos in the SN neutrino flux. This, however, needs a detailed analysis that is beyond the scope of this short review.

Finally, it may be possible to experimentally measure the energy spectrum of the emitted neutrons. The theoretically calculated spectrum turns out to be sim-

[1] The proposed 50 kton magnetized Iron Calorimeter (ICAL) detector to be located at the proposed India-based Neutrino Observatory (INO) is designed primarily for the study of neutrino properties, in particular, the neutrino mass hierarchy, using atmospheric neutrinos, and was originally not designed to be sensitive to much lower energy SN neutrinos. However, it can in principle be modified with suitably placed layers of neutron detectors to make the detector sensitive to SN neutrino induced neutrons.

Table 2 Number of neutrons (N_n) emitted per kton of different detector materials along with the cumulative total number (Sum) as a function of ν_e energy (in 5 MeV bins) due to CC interactions of the SN-ν_es, for the case of Normal Ordering (NO) of neutrino masses, with the corresponding numbers for the Inverse Ordering (IO) given in parentheses

E_ν	^{56}Fe		^{132}Xe		^{208}Pb	
(MeV)	N_n	Sum	N_n	Sum	N_n	Sum
0–5	0.0	0.0	0.0	0.0	0.0	0.0
	(0.0)	(0.0)	(0.0)	(0.0)	(0.0)	(0.0)
5–10	0.0	0.0	0.01	0.01	0.0	0.0
	(0.0)	(0.0)	(0.0)	(0.0)	(0.0)	(0.0)
10–15	0.04	0.04	0.77	0.78	2.24	2.24
	(0.04)	(0.04)	(0.84)	(0.84)	(2.63)	(2.63)
15–20	0.23	0.27	7.38	8.16	12.44	14.68
	(0.21)	(0.25)	(6.73)	(7.57)	(11.91)	(14.54)
20–25	0.46	0.73	18.13	26.29	25.79	40.47
	(0.38)	(0.63)	(13.80)	(21.37)	(21.06)	(35.60)
25–30	0.54	1.27	23.33	49.62	31.54	72.01
	(0.41)	(1.04)	(17.62)	(38.99)	(23.59)	(59.19)
30–35	0.51	1.78	21.34	70.98	27.30	99.31
	(0.36)	(1.40)	(15.36)	(54.35)	(19.23)	(78.42)
35–40	0.43	2.21	16.17	87.15	21.02	120.33
	(0.31)	(1.71)	(11.37)	(65.72)	(14.34)	(92.76)
40–45	0.35	2.56	10.87	98.02	14.74	135.07
	(0.25)	(1.96)	(7.56)	(73.28)	(9.98)	(102.74)
45–50	0.27	2.83	6.74	104.76	9.38	144.45
	(0.19)	(2.15)	(4.67)	(77.95)	(6.15)	(108.89)
50–55	0.20	3.03	3.95	108.71	5.32	149.77
	(0.14)	(2.29)	(2.73)	(80.68)	(3.91)	(112.80)
55–60	0.14	3.17	2.22	110.93	3.30	153.07
	(0.10)	(2.39)	(1.53)	(82.21)	(2.06)	(114.86)

The numbers are for SN neutrino flux as given by the Basel/Darmstadt simulations [24] of a 18 $M_\odot$ progenitor supernova at a distance of 10 kpc. The numbers for ^{56}Fe and ^{208}Pb are from Ref. [22] and those for ^{132}Xe are from Ref. [23]

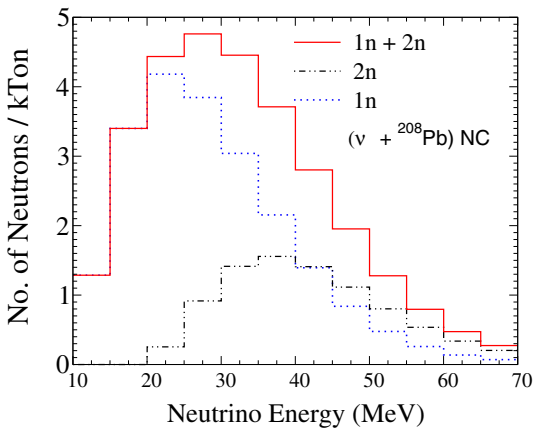

Fig. 5 Number of neutrons emitted as a function of neutrino energy by NC excitation of ^{208}Pb for SN neutrino flux given by the Basel/Darmstadt simulations [24] of a 18 $M_\odot$ progenitor supernova at a distance of 10 kpc. (From [22])

ilar for all the three cases of nuclei with very different masses. For illustration, we give in Fig. 6 the energy spectrum of neutrons emitted by ^{132}Cs due to CC interaction of the SN ν_es with the nucleus ^{132}Xe, for SN neutrino flux given by the Basel/Darmstadt simulations [24] of a 18 $M_\odot$ progenitor supernova at a distance of 10 kpc. The emitted neutrons are seen to reach a peak at around 1.5 MeV and then fall off becoming very small beyond 7 MeV or so.

6 Summary and outlook

In this article, we have given a brief review of supernova neutrino induced neutron production in different detector materials with primary focus on reviewing the nuclear physics aspects of neutrino induced nuclear excitation and subsequent de-excitation of the nuclei through neutron emission. We have used the simulation results of the Basel/Darmstadt group for the explosion of a 18 $M_\odot$ progenitor star at a distance of 10 kpc for illustrating our results for neutron production in different detector materials.

We have noted that the number of neutrons produced differs for the two different neutrino mass orderings, i.e., normal- and inverted ordering. While this raises the tantalizing possibility of distinguishing between the two mass hierarchies through detection of the SN neutrino-induced neutrons, this will probably be an extremely difficult task given the currently uncertain physics of

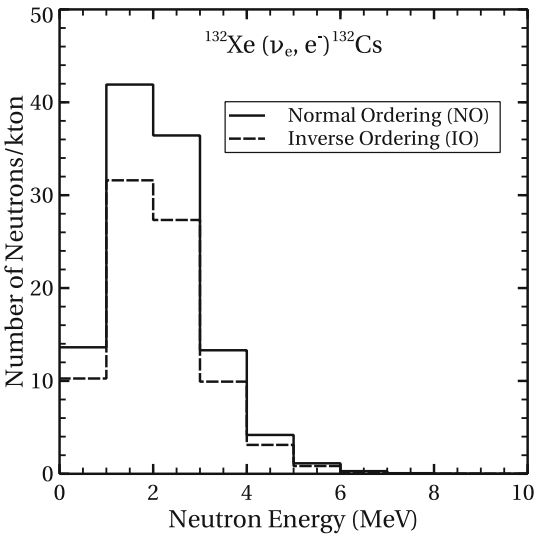

Fig. 6 Spectrum of neutrons emitted by ^{132}Cs excited by SN neutrinos through the CC process $^{132}\mathrm{Xe}\,(\nu_e, e^-)^{132}\mathrm{Cs}$ for both NO and IO cases, for SN neutrino flux given by the Basel/Darmstadt simulations [24] of a 18 $\mathrm{M}_\odot$ progenitor supernova at a distance of 10 kpc. (From [23])

flavor conversion within the supernova and the resulting uncertainties in the source spectrum of neutrinos.

Perhaps more useful from the standpoint of experimental exploration is our observation that while the dominant fraction of neutrons produced in neutron-rich materials such as lead comes from charged current interaction of the ν_es, the opposite happens in a low-neutron excess material such as iron for which the neutrons produced by the combined neutral current interactions of all the six neutrino plus antineutrino species dominate. We propose that this complementarity between high- and low-neutron excess detector materials may offer a way of estimating the fraction of mu- and tau flavored neutrinos (which interact only through neutral current) in the total SN neutrino flux by means of simultaneous detection of a SN through the neutron channel in two sufficiently large detectors, with one detector made of lead (high neutron excess) and the other of iron (low neutron excess), for example. This can give valuable information about the production and flavor oscillation processes of neutrinos in supernovae. Of course, the amounts of detector material that will be needed for each type of detector for drawing statistically significant inference on the flavor composition of the SN neutrinos will require a detailed analysis that is beyond the scope of the present article.

In the above discussion, we have used a specific set of simulation results, namely, that of the Basel/Darmstadt group for the explosion of a 18 $\mathrm{M}_\odot$ progenitor star. It will be important to use the results of other simulations that include more realistic mean field and modification of the symmetry energy as pointed out in recent works, and also consider different masses of the progenitor star to have a better idea of the systematic uncertainties in the prediction of number of neutrons produced. Finally, one hopes that a future core collapse supernova will be observed at a distance closer than 10 kpc; an explosion at a distance of 1 kpc, for example, will give 100 times more events than what we have estimated here.

We thank Abhijit Bandyopadhyay, Sovan Chakraborty and Satyajit Saha for helpful discussions. One of us (PB) acknowledges support under a Raja Ramanna Fellowship of the Dept. of Atomic Energy, Govt. of India.

Author contribution statement

Both the authors have contributed equally to the preparation of the first draft and subsequent modifications leading to the final version of the manuscript.

References

1. H.A. Bethe, Rev. Mod. Phys. **62**, 801 (1990)
2. H-Th Janka, K. Langanke, A. Marek, G. Martinez-Pinedo, B. Mueller, Phys. Rep. **442**, 38 (2007)
3. K. Scholberg, Ann. Rev. Nucl. Part. Sci. **62**, 81 (2012)
4. G.G. Raffelt, Ann. Rev. Nucl. Part. Sci. **49**, 163 (1999)
5. H. Duan, J.P. Kneller, J. Phys. G **36**, 113201 (2009)
6. K. Hirata et al., (KAMIOKANDE-II Collaboration), Phys. Rev. Lett. **58**, 1490 (1987)
7. R.M. Bionta, G. Blewitt, C.B. Bratton, D. Casper, A. Ciocio, R. Claus, B. Cortez, M. Crouch et al., Phys. Rev. Lett. **58**, 1494 (1987)
8. K. Abe et al. (Super-Kamiokande), Phys. Rev. D **83**, 052010 (2011)
9. R. Abbasi et al., (IceCUBE), Astron. Astrophys. **535**, A109 (2011)
10. L. Cadonati, F.P. Calaprice, M.C. Chen, Astropart. Phys. **16**, 361 (2002)
11. V.D. Berger, D. Marftia, B.P. Wood, Phys. Lett. B **498**, 53 (2001)
12. K. Asakura et al. (KamLAND), Astrophys. J. **818**, 91 (2016)
13. N.Y. Agafonova et al. (LVD), Astrophys. J. **802**, 47 (2015)
14. S.B. Kim, Nucl. Part. Phys. Proc. **265–266**, 93 (2015)
15. M.G. Aartsen et al., (ICECUBE) (2014) arXiv:1412.5106
16. K. Abe et al. (2011) arXiv:1109.3262
17. F. An et al. (JUNO), J. Phys. G **43**, 030401 (2016)
18. R. Acciari et al. (DUNE) (2015) arXiv:1512.06148
19. J. Engel, G.C. McLaughlin, C. Volpe, Phys. Rev. D **67**, 013005 (2003)
20. C.A. Duba et al., J. Phys. Conf. Ser. **136**, 042077 (2008)
21. E. Kolbe, K. Langanke, Phys. Rev. C **63**, 025802 (2001)
22. A. Bandyopadhyay, P. Bhattacharjee, S. Chakraborty, K. Kar, S. Saha, Phys. Rev. D **95**, 065002 (2017)
23. P. Bhattacharjee, A. Bandyopadhyay, S. Chakraborty, S. Ghosh, K. Kar, S. Saha (2020). arXiv:2012.13986v2
24. T. Fischer, S.C. Whitehouse, A. Mezzacappa, F.-K. Thielemann, M. Liebendorfer, Astron. Astrophys. **517**, A80 (2010)
25. T. Totani, K. Sato, H.E. Dalhed, J.R. Wilson, Astrophys. J. **496**, 216 (1998)

26. M.T. Keil, G.G. Raffelt, H.-T. Janka, Astrophys. J. **590**, 971 (2003)
27. G. Martinez-Pinedo, T. Fischer, A. Lohs, L. Huther, Phys. Rev. Lett. **109**, 251104 (2012)
28. T. Fischer, Astron. Astrophys. **593**, A103 (2016)
29. See, e.g., R.N. Mohapatra and P.B. Pal, *Massive Neutrinos in Physics and Astrophysics*, 3rd Ed. (World Scientific, Singapore, 2004)
30. A.S. Dighe, AYu. Smirnov, Phys. Rev. D **62**, 033007 (2000)
31. H. Duan, G.M. Fuller, Y.-Z. Qian, Ann. Rev. Nucl. Part. Sci. **60**, 569 (2010)
32. A. Mirrizi, I. Tamborra, H.-T. Janka, N. Saviano, K. Scholberg, R. Bolig, L. Hudepohl, S. Chakraborty, Riv. Nuovo Cim. **39**, 1 (2016)
33. N. Saviano, S. Chakraborty, T. Fisher, A. Mirizzi, Phys. Rev. D **85**, 113002 (2012)
34. S. Chakraborty, T. Fischer, A. Mirizzi, N. Saviano, R. Tomas, Phys. Rev. Lett. **107**, 151101 (2011)
35. S. Chakraborty, T. Fischer, A. Mirizzi, N. Saviano, R. Tomas, Phys. Rev D **84**, 025002 (2011)
36. T. Kuramoto, M. Fukugita, Y. Kohyama, K. Kubodera, Nucl. Phys. A **512**, 711 (1990)
37. G.M. Fuller, W.C. Haxton, G.C. McLaughlin, Phys. Rev. D **59**, 085005 (1999)
38. E. Kolbe, K. Langanke, G. Martinez-Pinedo, Phys. Rev. C **60**, 052801 (1999)
39. J. Engel, Phys. Rev. C **57**, 2004 (1998)
40. E. Caurier, K. Langanke, G. Martinez-Pinedo, F. Nowacki, Nucl. Phys. A **653**, 439 (1999)
41. K. Langanke, D.J. Dean, P.B. Radha, Y. Alhasid, S.E. Koonin, Phys. Rev. C **52**, 718(1995)
42. T.T.S. Kuo, G.E. Brown, Nucl. Phys. A **114**, 241 (1968)
43. A. Poves, A.P. Zuker, Phys. Rep. **70**, 235 (1981)
44. P. Sarriguren, E. Moya de Guerra, A. Escuderos, A.C. Carrizo, Nucl. Phys. A **635**, 55 (1998)
45. O. Moreno, R. Alvarez-Rodriguez, R. Sarriguren, E. Moya de Guerra, J.M. Udias, J.R. Vignote, Phys. Rev. C **74**, 054308 (2006)
46. O.B. Tarasov, D. Bazin, Nucl. Instrum. Meth. B **204**, 174 (2003). http://lise.nscl.msu.edu/pace4.html
47. A. Gavron, Phys. Rev. C **21**, 230 (1980)
48. See, for a review, T.M. Undagoitia and L. Rauch, J. Phys. G: Nucl. Part. Phys. **43**, 013001 (2016). arXiv:1509.08767
49. S. Chakraborty, P. Bhattacharjee, K. Kar, Phys. Rev. D **89**, 013001 (2014)
50. R.F. Lang, C. McCabe, S. Reichard, M. Selvi, I. Tamborra, Phys. Rev. D **94**, 103009 (2016)
51. D.Z. Freedman, Phys. Rev. D **9**, 1389 (1974)
52. D.Z. Freedman, D.N. Schramm, D.L. Tubbs, Ann. Rev. Nucl. Part. Sci. **27**, 167 (1977)
53. C.J. Horowitz, K.J. Coakley, D.N. McKinsey, Phys. Rev. D **68**, 023005 (2003)
54. S. Ünlü, H.A. Aygör, N. Çakmak, C. Selam, Turk. J. Phys. **40**, 304 (2016)
55. R. Lazauskas, C. Volpe, Nucl. Phys. A **792**, 219 (2007)
56. N. Paar, D. Vretenar, P. Ring, J. Phys. G **35**, 014058 (2008)
57. The ICAL Collaboration: A. Kumar et al., Pramana J. Phys **88**, 79 (2017)
58. S. Ahmed et al, arXiv:1505.07380v2